Modeling Molecular Weight and Degree of Branching Distribution of Low-Density Polyethylene

Piet D. Iedema,*,† Michael Wulkow,‡ and Huub C. J. Hoefsloot†

Department of Chemical Engineering, Universiteit van Amsterdam, Amsterdam, The Netherlands; and Computing in Technology GmbH, Rastede, Germany

Received October 13, 1999; Revised Manuscript Received June 19, 2000

ABSTRACT: A new strategy for the simultaneous modeling of molecular weight distribution (MWD) and degree of branching distribution (DBD) for such branched polymers as bimodal low-density polyethylene is presented, based on the Galerkin h−p finite element package PREDICI, a commercial code. The key problem of how to address a bidimensional distribution is successfully solved by using so-called reduced or pseudo distributions. The branching distribution per chain length is modeled by moment equations, thus yielding distributions of branching moments over chain length. No closure relationships are required. The MWD/DBD curves obtained are the most probable ones for the given reaction mechanisms and kinetic data. Simulated MWD and DBD curves are compared to experimental data from gel permeation chromatography and light scattering; the agreement found is good in general and excellent in one case. The bimodal MWD of the autoclave low-density polyethylene (ldPE) IUPAC Alpha could be reproduced well. It is finally shown that the shapes of MWD and DBD are highly sensitive, quantitative measures for random scission.

Introduction

Scope. Control of microstructural properties of low-density polyethylene in reactors is an issue of high industrial importance. Although the process is one of the oldest commercial radical polymerization systems, it still presents scientific challenges. The issue is to find the relationship between ldPE reactor conditions and the complex microstructure of various grades of this polymer. This paper focuses on two interrelated aspects of this structure: The molecular weight distribution (MWD) and the degree of branching distribution (DBD). The highly desired quality of some autoclave grades of ldPE is ascribed to the broad, shouldered MWD and the presence of long branches especially at the higher MW tail. This observation is based on MWD and DBD data obtained by means of characterization techniques, which over the past decade have become not only practically, but also scientifically reliable. Hence, in principle, such data are technically accessible, which does not automatically imply that they are abundantly available from nonconfidential sources. Only one recent publication[1] containing MWD and DBD data—the key reference for our modeling work—exists, while other available data are relatively old or incomplete.[2−6]

It should be noted that MWD and DBD are closely related. Branches are mainly created by a transfer to polymer reaction. Since this is a process in which dead chains are reactivated and again grow by propagation, branching is accompanied by molecular mass increase. A second link between MWD and DBD originates in the characterization of the polymer. The MWD is determined from size exclusion chromatography (SEC), but has to be corrected for the degree of branching. Hence, knowledge about branching is a precondition for the exact MWD determination. Therefore, if studies are devoted to full MW distributions, it is relevant to make reference explicitly to the branching issue.

* To whom correspondence should be addressed at the Universiteit van Amsterdam.
† Universiteit van Amsterdam.
‡ Computing in Technology GmbH.

Previous Work. Modeling devoted to MW and MWD of ldPE has been performed by several authors, who used the method of moments, or more sophisticated or detailed techniques, i.e., continuous variable approximation, Monte Carlo simulations, and/or finite element methods.[11−16,20,23−30,33,35] Full MW distributions are mostly obtained from the last-mentioned class of techniques, but the typical bimodal MWD with polydispersity around 25 of autoclave ldPE[1] has never been reproduced by models in the open literature. In the history of ldPE modeling, the incorporation of the random scission came relatively late.[33] More recently, the mechanism has been adopted by most authors, except—somewhat surprisingly—Nordhus et al.,[6] who use a continuous-variable approximation. This is probably due to problems encountered by modeling random scission as one of the most difficult reaction steps.

Most recently—and to our knowledge, for the first time—the MWD and DBD issues have been addressed in a moment modeling study of ldPE in continuously stirred tank reactors (CSTR).[20] Here, the concept of numerical fractionation[23] has been applied, with branch number classes representing the fractions. Quite interestingly, for very high transfer to polymer rates, an MWD of polydispersity 4.5 was computed to have a bimodal shape when scaled with nP_n. Note that SEC provides data on a n^2P_n scale instead. The computed DBD proved to be in the same order of magnitude as experimental data,[5] although here a calculated CSTR result was compared to the measured tubular product NBS 1476. The moment method may not always be adequate for describing such complex systems as ldPE, which require closure relations and the translation of moments to full distributions that may introduce some arbitrariness.

The effect of reactor segregation on MWD has been raised[20] and indeed shows some influence in the case of autoclave reactors. We have performed compartment modeling using four CSTRs with recirculation,[13] but the results clearly indicate that, for autoclave conditions,

10.1021/ma991711o CCC: $19.00
Published on Web 09/01/2000

this yields only minor differences as compared to the single CSTR. However, the situation is completely different for ldPE from tubular reactors, since observed broad MWDs and branching distributions have not yet been explained by our model without assuming significant segregation. This needs to be investigated more thoroughly.

DBD has been modeled several times,[25−28] and especially the scission of branched molecules is highly interesting. It has been shown to be possible[25] to obtain the complete spatial structure of individual macromolecules, including the location of the branch points, which allows calculation of the exact radius of gyration of the branched molecule. This yields a direct link to the size of the molecule, as discussed in the next section, which is experimentally observable.

A New Approach. Since it is known that the method of moments encounters problems with closure relationships and that Monte Carlo simulations are accurate but too computationally intensive to describe reactors, an intermediate modeling strategy is required for our purpose as described above. This strategy is based on the Galerkin h−p method employed in the PREDICI package,[31] a commercial code. The present version of PREDICI allows one to deal with arbitrary systems of unidimensional models and distributions without applying closing relations. Consequently, this algorithm has been successfully applied several times to the modeling of MWDs of ldPE.[11−13] However, the simultaneous description of MWD and DBD leads to a bidimensional problem with the property coordinates *chain length* and *number of branches*. To avoid the computationally expensive bidimensional problem, a mathematical reduction technique is applied to the original model, which allows the computation of average branching degrees per chain length (and the respective variances). For that reason, *branching moment distributions* are introduced. The population balances for these distributions can be solved in PREDICI since they are unidimensional. Thus, the original bidimensional problem is replaced by a series of unidimensional problems with getting exact information on averages concerning the second distribution. The derivation of the extended balance equations for all reaction mechanisms involved will be given in this paper.

Kinetics

The reaction mechanisms are listed in Table 1. Macromolecular species are indexed by n—the chain length—and i, the number of branches per chain. Hence, P_n^i denotes the concentration of dead chains with length n and number of branches i; similarly, living chains are denoted by R_n^i. As indicated in Table 1, both indices can change upon reaction. The changes in n are as usual, and the changes in i will be explained in the section on modeling.

The reaction mechanisms selected are the ones mostly assumed to be involved in ldPE systems, and the rate constants are numerically almost identical to those in previous work.[15,20] A mechanism disregarded by us, but sometimes taken into account,[20] is that involving terminal double bonds. We checked the role of this mechanism by incorporating it in the same simplified way as the authors mentioned, and saw negligible influence on DB and none at all on MW. However, modeling this reaction in a more rigorous way—by taking into account populations of macroradicals carrying two or more radical centers, while maintaining the same rate constant—gave rise to a dramatic effect on MWD and DBD. Since no explicit experimental evidence supports this mechanism, we dropped it from the analysis. Finally, we assumed conversion and chain length to be independent termination reactions, although some dependence is probable. Some exploratory computational exercises concerning chain length dependent termination have shown that this affects to some extent the shape of the MWD. For the time being, we consider this a refinement of minor importance for ldPE, and it will be revisited for other systems in future studies.

Table 1. Presumed Reaction Mechanisms in Bidimensional Notation: Lower Case Index Denotes Chain Length; Upper Case Index Denotes Number of Branches

initiation	$I_2 \xrightarrow{k_d} 2I\bullet$
	$I\bullet \xrightarrow{k_1^*\eta_I} R_1\bullet$
propagation	$R_n^{\,i}\bullet + M \xrightarrow{k_p} R_{n+1}^{\,i}\bullet$
termination *combination*	$R_n^{\,i}\bullet + R_m^{\,j}\bullet \xrightarrow{k_{tc}} P_{n+m}^{i+j}$
termination *disproportionation*	$R_n^{\,i}\bullet + R_m^{\,j}\bullet \xrightarrow{k_{td}} P_n^{\,i} + P_m^{\,j}$
chain transfer (CT) to monomer	$R_n^{\,i}\bullet + M \xrightarrow{k_m} P_n^{\,i} + R_1\bullet$
CT to chain transfer agent	$R_n^{\,i}\bullet + S \xrightarrow{k_S} P_n^{\,i} + R_1\bullet$
CT to polymer	$R_n^{\,i}\bullet + P_m^{\,j} \xrightarrow{k_{tp}^*m} P_n^{\,i+1} + R_m^{\,j}\bullet$
random scission	$R_n^{\,i}\bullet + P_m^{\,j} \xrightarrow{k_{rs}^*m} P_n^{\,i} + P_{m-r}^{j-k} + R_r^{\,k}\bullet$

The role of random scission—being the most recently introduced mechanism in the history of ldPE modeling[33]—is a special one. This mechanism is distinct from β-scission, which takes place at chain ends and leads to short chain branches. Our study disregards β-scission, since we are interested in long chain branches and also because the MWD is not affected by β-scission. Random scission chiefly has an impact on the way the MWD is broadened by transfer to polymer, as will be shown at the end of this article. In the absence of random scission, the polydispersity for these radical systems in a CSTR turns out to have a maximum of only 3.5, which is much lower than the reported values. Finally, the assumption of randomness in the scission reaction modeled—every bond in the macromolecule is equally likely to break—may be a matter of dispute. The scission of branched chains is known to be a complex problem.[27] However, we will start with this most simple scheme and see how it works out on the MWD and DBD for a relevant range of the associated rate constant k_{rs}.

MWD and DBD Modeling with PREDICI

The Bidimensional Character of the Problem. It is clear from the reaction mechanisms that the problem is a bidimensional one, or that P_n^i and R_n^i are bidimensional distributions. These are related to the usual unidimensional concentrations and moments by summing over the branching index i:

$$R_n = \sum_{i=0}^{\infty} R_n^i, \quad P_n = \sum_{i=0}^{\infty} P_n^i \tag{1}$$

$$\text{living chains: } \lambda_N = \sum_{n=1}^{\infty} n^N R_n; \qquad \text{dead chains: } \mu_N = \sum_{n=2}^{\infty} n^N P_n \quad (2)$$

The total concentration of branch points B is then expressed by

$$B = \sum_{n=2}^{\infty}\sum_{i=0}^{\infty} i P_n^i \quad (3)$$

According to the chemical interpretation, the number of branches should be equal to the number of times a chain undergoes a transfer to polymer reaction, since every such reaction leads to a branch, except for terminal units. Thus, a simple relation exists between the kinetic rate constant and the total concentration of branches

$$\frac{\mathrm{d}B}{\mathrm{d}t} = k_{tp}\lambda_0\mu_1 \quad (4)$$

where statistical moments of living (λ_0) and dead (μ_1) polymer are used. Hence, in principle, the transfer coefficient k_{tp} may be obtained from measured branching data. However, it should be borne in mind that, in practice, the total number of branches is not directly determined by counting the individual branching reactions, nor by visual observation of the number of branch points in all the molecules.[25] Instead, the degree of branching is determined indirectly from information about the size (distribution) of the molecules, and [henceforth = therefore?] always involves some way of averaging in the bidimensional domain.

Using Pseudo Distributions To Deal with Multidimensionality. In this section, the problem of how to manage multidimensionality with a unidimensional algorithm will be addressed. PREDICI[31] is based on a finite element Galerkin h−p scheme combined with a special time discretization of Rothe's type. It computes full MW distributions from basic kinetic schemes and data without any further assumptions or closure relations. At present, PREDICI is limited to systems of unidimensional distributions, while the presented problem is bidimensional—chain length and branches per chain being the property coordinates of the distribution P_n^i. The most rigorous way to deal with this would be to extend PREDICI to two dimensions, but such an extension is not yet available. For this reason, a new concept using *reduced* (or *pseudo*) *distributions* has been developed, based on the unidimensional algorithm.

The basic idea is that in systems with more than one property coordinate (variable), in many cases the full multidimensional information cannot be obtained or is not interesting. Thus, one applies a certain kind of averaging over some of the coordinates. This is widely used in statistical physics and also has applications in chemical engineering. However, a systematic approach to models in polymer chemistry has not yet been developed. A reason for this may be that the arising extended population balances are even more complicated than the typical balances describing molecular weight distributions. However, this is not an obstacle in view of the application of the Galerkin h−p method. A detailed overview and more applications will be presented in forthcoming papers; in particular, a comparison with Monte Carlo simulations is in progress.

Starting from the bidimensional distributions for dead and living chains P_n^i and R_n^i, respectively, in the present context reduced distributions are defined as follows:

$$\text{dead chains:} \quad \Psi_n{}^N = \sum_{i=0}^{\infty} i^N P_n^i \quad (5)$$

$$\text{living chains:} \quad \Phi_n{}^N = \sum_{i=0}^{\infty} i^N R_n^i \quad (6)$$

From these Nth branching moment distributions, averages may be derived. For example, the average number of branches of chains of length n can be computed by the ratio (for each n) of the first and zeroth branching moment distribution. Note that $\Psi_n{}^0$ equals P_n. To derive the balance equations for the branching moment distributions, the following steps have to be performed:

- Deriving the bidimensional population balance for each reaction step of the kinetic model.
- Reducing the bidimensional balance to a unidimensional balance, by applying the above summations over the branching index (same type of operation as obtaining moments from distributions).
- Expressing the resulting terms in terms of the branching moment distributions, and then adding them to the system of equations.

All equations are simultaneously solved in PREDICI. This procedure can principally be applied to any polyreaction model where additional properties have to be considered. The key is how a certain reaction step changes the additional property. In the present case, the branching index is mainly affected by transfer to polymer, scission, and termination.

Population Balances for Branching Moment Distributions. In this section, the balance equations for all reaction mechanisms involved will be derived and presented per mechanism as contributions to the overall balances. Reactions not affecting the number of branches per chain—i.e., those describing propagation, transfer to monomer, and solvent and termination by disproportionation—will be presented in the first part. The reactions which do affect branching—i.e., transfer to polymer, termination by combination, and random scission—are more complex and will be discussed subsequently. The distributions of the original kinetic model will be called *real* distributions, and the additional branching moment distributions will be called *pseudo* distributions. Note that the += duet means *a contribution to* the overall balance equation of the respective species.

Propagation Step.

$$\text{reaction mechanism: } R_n{}^i + M \xrightarrow{k_p} R_{n+1}{}^i$$

In this case, the degree of branching is not altered; hence, this is a simple step from this point of view. The living chain balance in bidimensional notation is

$$\frac{\mathrm{d}R_n{}^i}{\mathrm{d}t} \mathrel{+}= k_p M(-R_{n-1}{}^i + R_n{}^i) \quad (7)$$

The contribution to the balance of the Nth branching moment distributions of living chains in reduced or pseudo distribution notation follows by multiplication

with i^N and taking the summation over the branching index i:

$$\frac{d\Phi_n{}^N}{dt} = \sum_{i=0}^{\infty} i^N \left(\frac{dR_n{}^i}{dt}\right) += k_p M(-\Phi_{n-1}{}^N + \Phi_n{}^N) \quad (8)$$

Transfer to Monomer and Solvent Reactions.

$$R_n{}^i + M \xrightarrow{k_m} P_n{}^i + R_1; \quad R_n{}^i + S \xrightarrow{k_s} P_n{}^i + R_1$$

We can neglect the production of monomer radicals, since these do not carry branches. Again, the degree of branching is not affected; hence, the contributions to the pseudo distribution balances of the living and dead chains are

$$\frac{d\Phi_n{}^N}{dt} += -k_m M\Phi_n{}^N; \quad \frac{d\Psi_n{}^N}{dt} += k_m M\Phi_n{}^N \quad (9)$$

Termination by Disproportionation.

$$R_n{}^i + R_m{}^j \xrightarrow{k_{td}} P_n{}^i + P_m{}^j$$

The contribution to the balance of the living and dead chains $R_n{}^i$ and $P_n{}^i$, are the same but of opposite sign, and again they do not involve any change of degree of branching:

$$\frac{dR_n{}^i}{dt} = -\frac{dP_n{}^i}{dt} += -k_{td}R_n{}^i \sum_{n=1}^{\infty}\sum_{i=0}^{\infty} R_n{}^i = -k_{td}R_n{}^i\lambda_0 \quad (10)$$

Contributions to the balances of the pseudo distributions again follow after multiplying with i^N and summation over i as

$$\frac{d\Phi_n{}^N}{dt} = -\frac{d\Psi_n{}^N}{dt} += -k_{td}\Phi_n{}^N\lambda_0 \quad (11)$$

Termination by combination. This reaction mechanism is somewhat more complicated, since a change of the branching index is involved:

$$R_n{}^i + R_m{}^j \xrightarrow{k_{tc}} P_{n+m}^{i+j}$$

The lengths n and m and the degrees of branching i and j of the living chains R are added in the dead chain P produced by combination. Since this reaction only consumes living chains, the corresponding bidimensional balance for $R_n{}^i$ is still simple:

$$\frac{dR_n{}^i}{dt} += -k_{tc}R_n{}^i \sum_{n=1}^{\infty}\sum_{i=0}^{\infty} R_n{}^i = -k_{tc}R_n{}^i\lambda_0 \quad (12)$$

This expression has exactly the same shape as eq 10 for disproportionation, and consequently yields a reduced balance of the same shape as eq 11:

$$\frac{d\Phi_n{}^N}{dt} += -k_{tc}\Phi_n{}^N\lambda_0 \quad (13)$$

The bidimensional expression for the contribution of the combination reaction to the balance for dead chains $P_n{}^i$ is more complex and contains the double summation over n and i

$$\frac{dP_n{}^i}{dt} += \frac{1}{2}k_{tc}\sum_{m=1}^{n-1}\sum_{j=0}^{i}(R_m{}^j R_{n-m}^{i-j}) \quad (14)$$

Multiplying with i^N and summation over i again produces the reduced expression for this balance in terms of the Nth branching moment distribution of dead chains:

$$\frac{d\Psi_n{}^N}{dt} += \frac{1}{2}k_{tc}\sum_{i=0}^{\infty} i^N \left(\sum_{m=1}^{n-1}\sum_{j=0}^{i} R_m{}^j\, R_{n-m}^{i-j}\right) \quad (15)$$

For $N = 1$, eq 15 can be rearranged in the following way:

$$\begin{aligned}\frac{d\Psi_n{}^1}{dt} += \frac{1}{2}k_{tc}\sum_{i=0}^{\infty} i\left(\sum_{m=1}^{n-1}\sum_{j=0}^{i} R_m{}^j R_{n-m}^{i-j}\right) = \\ \frac{1}{2}k_{tc}\sum_{m=1}^{n-1}\sum_{j=0}^{\infty} R_m{}^j\left(\sum_{i=j}^{\infty} i R_{n-m}^{i-j}\right) = \\ \frac{1}{2}k_{tc}\sum_{m=1}^{n-1}\sum_{j=0}^{\infty} R_m{}^j\left(\sum_{i=0}^{\infty}(i+j)R_{n-m}^{i}\right) = \\ \frac{1}{2}k_{tc}\sum_{m=1}^{n-1}\left(\sum_{j=0}^{\infty} jR_m^j\sum_{i=0}^{\infty} R_{n-m}^{i} + \sum_{j=0}^{\infty} R_m{}^j\sum_{i=0}^{\infty} iR_{n-m}^{i}\right) = \\ \frac{1}{2}k_{tc}\sum_{m=1}^{n-1}(\Phi_m{}^1 R_{n-m} + R_m\Phi_{n-m}^1) = k_{tc}\sum_{m=1}^{n-1}\Phi_m{}^1 R_{n-m}\end{aligned} \quad (16)$$

Note that this expression is similar to the well-known *first* moment equation for combination in one dimension (chain length) containing the product of zeroth and first living chain moments $\lambda_1\lambda_0$. Equation 16 contains the product $\Phi_m{}^1 R_{n-m}$ under the summation sign, and knowing that R_n may be interpreted as the zeroth moment of $\Phi_n{}^N$, the product term can also be read as $\Phi_m{}^1\Phi_{n-m}{}^0$, which shows the resemblance to the moment product $\lambda_1\lambda_0$.

The contribution to the second branching moment distribution of dead chains is obtained by a similar transformation of eq 16:

$$\begin{aligned}\frac{d\Psi_n{}^2}{dt} += \frac{1}{2}k_{tc}\sum_{i=0}^{\infty} i^2\left(\sum_{m=1}^{n-1}\sum_{j=0}^{i} R_m{}^j R_{n-m}^{i-j}\right) = \\ \frac{1}{2}k_{tc}\sum_{m=1}^{n-1}\sum_{j=0}^{\infty} R_m{}^j\left(\sum_{i=0}^{\infty}(i+j)^2\, R_{n-m}^{i}\right) = \\ \frac{1}{2}k_{tc}\sum_{m=1}^{n-1}(\Phi_m{}^2 R_{n-m} + 2\Phi_m{}^1\Phi_{n-m}^1 + R_m\Phi_{n-m}^2) = \\ k_{tc}\sum_{m=1}^{n-1}(\Phi_m{}^2 R_{n-m} + \Phi_m{}^1\Phi_{n-m}^1)\end{aligned} \quad (17)$$

This time a similarity to the usual *second* moment balance equation is seen, which contains the term $\lambda_2\lambda_0 + \lambda_1{}^2$ which compares well with the last term under the summation in eq 17.

Transfer to Polymer. This reaction is interesting, since in our model branches are generated by this mechanism only. The mechanism adds one to the degree of branching of existing dead chains $P_m{}^j$, the index j becoming $j + 1$:

$$R_n^i + P_m^j \xrightarrow{k_{tp}m} P_n^i + R_m^{j+1}$$

Concerning the living chain balance, we see that according to the left-hand side of this reaction, equation chains of index i are consumed, but according to the right-hand side, chains of index $j + 1$ (i) are produced from dead chains of one index lower j ($i - 1$). Hence, the contribution to the bidimensional living chain balance becomes:

$$\frac{dR_n^i}{dt} += k_{tp}(-\mu_1 R_n^i + \lambda_0 n P_n^{i-1}) \quad (18)$$

The reduced form of this expression follows after multiplying with i^N and summing over i:

$$\frac{d\Phi_n^N}{dt} += k_{tp}(-\mu_1 \Phi_n^N + \lambda_0 n \sum_{i=0}^{\infty} i^N P_n^{i-1}) \quad (19)$$

The first reduced moment balance follows by taking $N = 1$:

$$\frac{d\Phi_n^1}{dt} += k_{tp}(-\mu_1 \Phi_n^1 + \lambda_0 n \sum_{i=0}^{\infty} i P_n^{i-1}) = k_{tp}\{-\mu_1 \Phi_n^1 + \lambda_0 n(\Psi_n^1 + P_n)\} \quad (20)$$

Note here the appearance of P_n in the right-hand side of this expression, which can be interpreted as the zeroth moment of the dead chains Ψ_n^0. It means that the first branching moment of the living chains depends on the zeroth branching moment of the dead chains, which is the logical consequence of the index increase. Similarly, for $N = 2$ the second reduced moment balance follows:

$$\frac{d\Phi_n^2}{dt} += k_{tp}(-\mu_1 \Phi_n^2 + \lambda_0 n \sum_{i=0}^{\infty} i^2 P_n^{i-1}) = k_{tp}\{-\mu_1 \Phi_n^1 + \lambda_0 n(\Psi_n^2 + 2\Psi_n^1 + P_n)\} \quad (21)$$

This time, the right-hand side contains both lower moments Ψ_n^1 and Ψ_n^0 (P_n), again as a consequence of the index change incurred by the transfer to the polymer reaction.

The contributions to the dead chain balance are described by simpler expressions, since consumption of P_n^i and production of dead chains P_n^i from R_n^i do not involve an index change. The bidimensional balance becomes

$$\frac{dP_n^i}{dt} += k_{tp}(\mu_1 R_n^i - \lambda_0 n P_n^i) \quad (22)$$

The reduced balance equations for the Nth moment can then simply be written as

$$\frac{d\Psi_n^N}{dt} += k_{tp}(\mu_1 \Phi_n^N - \lambda_0 n \Psi_n^N) \quad (23)$$

yielding the leading moment equations by putting $N = 1, 2, \ldots$.

Random Scission. The most general form of the reaction equation describing scission of a dead chain P_m^j at an arbitrary bond is given by

$$R_n^i + P_m^j \xrightarrow{k_{rs}m} P_n^i + R_{m-l}^{\beta(m,j,m-l,j-k)} + P_l^{\beta(m,j,l,k)}$$

The function $\beta(m,j,l,k)$ denotes the probability that a chain of length m with j branches upon scission will produce a fragment of length l with k branches. In general, this probability depends on all the characteristics of the original chain—m and j—and those of the fragment, l and k. To solve the problem, a functional form for β has to be found. Several alternatives are available, from which we have selected one based on the assumption that the number of branches of the fragments is independent of the lengths of the original chain and the fragments. Thus, the probability function becomes

$$\beta(m,j,l,k) = \frac{1}{j+1} \quad j \ll m,\ k \ll l \quad (24)$$

Now, the bidimensional living chain balance contribution from random scission contains a simple consumption term referring to the termination of a macroradical R_n^i into a dead chain P_n^i, and a more complex production term denoting the production of R_n^i by the scission reaction. A macroradical with length n and number of branches i may be the scission product of all dead chains with length $l > n$ and branches $k \geq i$. The construction of the balance proceeds after the following argument. The probability that a dead chain P_l^k will break into a living fragment with a length of exactly $n < l$ is $k_{rs}P_l^k$. The probability that this fragment will have exactly $i \leq k$ branches is $1/(k + 1)$. Hence, the overall probability that a dead chain P_l^k will break into a living fragment R_n^i is $k_{rs}\lambda_0 P_l^k/(k + 1)$. This, then, is the production rate of R_n^i, dR_n^i/dt, from dead chains P_l^k. Since R_n^i may be produced from dead chains of length l with any number of branches k between i and $k_{max}(l)$, the production rate summed up over these dead chains equals $k_{rs}\lambda_0 \sum_{k=i}^{k_{max}(l)} P_l^k/(k + 1)$. Finally, since R_n^i may be produced from any dead chain of length $l > n$, the total production rate is summed up from $n + 1$ to ∞, yielding the balance

$$\frac{dR_n^i}{dt} += k_{rs}\left\{-\mu_1 R_n^i + \lambda_0 \sum_{l=n+1}^{\infty} \sum_{k=i}^{k_{max}(l)} \left(\frac{P_l^k}{k+1}\right)\right\} \quad (25)$$

However, this formulation would require not only truncated sums (which in general is no problem), but also an additional relation between branching density and scission, which is unknown. We therefore replaced the upper limit of the second summation, allowing it to run to infinity, which yields

$$\frac{dR_n^i}{dt} += k_{rs}\left\{-\mu_1 R_n^i + \lambda_0 \sum_{l=n+1}^{\infty} \sum_{k=i}^{\infty} \left(\frac{P_l^k}{k+1}\right)\right\} \quad (26)$$

Since on average the number of branches per chain is much smaller than the number of monomer units, the error made by this procedure is expected to be significant only for short chains. In fact, the number of branches in small chain fragments is heavily overestimated. This effect is discussed in the Appendix, and is shown to lead to acceptably small errors.

The reduced balance equation for the Nth branching moment of living chains based on eq 26 follows as usual by multiplication with i^N and summing over i:

$$\frac{d\Phi_n^N}{dt} += k_{rs}\left\{-\mu_1\Phi_n^N + \lambda_0\sum_{i=0}^{\infty} i^N \sum_{m=n+1}^{\infty}\sum_{j=i}^{\infty}\left(\frac{P_n^j}{j+1}\right)\right\} \quad (27)$$

For $N = 1$ in eq 27 we obtain the first moment equation:

$$\frac{d\Phi_n^1}{dt} += k_{rs}\left\{-\mu_1\Phi_n^1 + \lambda_0 \sum_{i=0}^{\infty} i \sum_{m=n+1}^{\infty}\sum_{j=i}^{\infty}\left(\frac{P_n^j}{j+1}\right)\right\} \quad (28)$$

The summation term may be rearranged to give

$$k_{rs}\lambda_0 \sum_{i=0}^{\infty}\sum_{m=n+1}^{\infty}\sum_{j=i}^{\infty}\left(\frac{P_n^j}{j+1}\right) = k_{rs}\lambda_0 \sum_{m=n+1}^{\infty}\sum_{j=0}^{\infty}\left\{\frac{P_n^j}{j+1}\left(\sum_{i=0}^{j} i\right)\right\} = k_{rs}\lambda_0 \sum_{m=n+1}^{\infty}\sum_{j=0}^{\infty}\left\{\frac{P_n^j}{j+1}\frac{j(j+1)}{2}\right\} = \frac{1}{2}k_{rs}\lambda_0 \sum_{m=n+1}^{\infty}\sum_{j=0}^{\infty}(jP_n^j) = \frac{1}{2}k_{rs}\lambda_0 \sum_{m=n+1}^{\infty}\Psi_m^1 \quad (29)$$

Hence, we find for the living chain pseudo distribution

$$\frac{d\Phi_n^1}{dt} += k_{rs}\left\{-\mu_1\Phi_n^1 + \frac{1}{2}\lambda_0 \sum_{m=n+1}^{\infty}\Psi_m^1\right\} \quad (30)$$

Taking $N = 2$ in eq 27, the contribution to the second branching moment distribution balance living chains is found:

$$\frac{d\Phi_n^2}{dt} += k_{rs}\left\{-\mu_1\Phi_n^2 + \lambda_0 \sum_{i=0}^{\infty} i^2 \sum_{m=n+1}^{\infty}\sum_{j=i}^{\infty}\left(\frac{P_n^j}{j+1}\right)\right\} \quad (31)$$

Rearrangement of the last term gives

$$k_{rs}\lambda_0 \sum_{i=0}^{\infty} i^2 \sum_{m=n+1}^{\infty}\sum_{j=i}^{\infty}\left(\frac{P_n^j}{j+1}\right) = k_{rs}\lambda_0 \sum_{m=n+1}^{\infty}\sum_{j=0}^{\infty}\left\{\frac{P_n^j}{j+1}\left(\sum_{i=0}^{j} i^2\right)\right\} = k_{rs}\lambda_0 \sum_{m=n+1}^{\infty}\sum_{j=0}^{\infty}\left\{\frac{P_n^j}{j+1}\frac{j(j+1)\left(j+\frac{1}{2}\right)}{3}\right\} = k_{rs}\lambda_0 \sum_{m=n+1}^{\infty}\sum_{j=0}^{\infty}\left\{\frac{1}{3}j\left(j+\frac{1}{2}\right)P_n^j\right\} = k_{rs}\lambda_0 \sum_{m=n+1}^{\infty}\left\{\frac{1}{3}\Psi_m^2 + \frac{1}{6}\Psi_m^1\right\} \quad (32)$$

Hence we find

$$\frac{d\Phi_n^2}{dt} += k_{rs}\left\{-\mu_1\Phi_n^2 + \lambda_0 \sum_{m=n+1}^{\infty}\left(\frac{1}{3}\Psi_m^2 + \frac{1}{6}\Psi_m^1\right)\right\} \quad (33)$$

The bidimensional balance for the dead chains contains three terms: A negative term describing the consumption of dead chains P_n^i and two positive ones, one referring to the generation of P_n^i from living chains R_n^i and the other denoting their generation as scission products from larger dead chains:

$$\frac{dP_n^i}{dt} += k_{rs}\left\{\mu_1 R_n^i - (n-1)\lambda_0 P_n^i + \lambda_0 \sum_{m=n+1}^{\infty}\sum_{j=i}^{\infty}\left(\frac{P_m^j}{j+1}\right)\right\} \quad (34)$$

The production term with the double summation is identical to the corresponding term in the living chain balance (eq 26) and relies on the same assumption as before concerning the complete decoupling between scission of lengths and branching numbers.

Now, the contribution of random scission to the balance of Nth branching moment distributions of dead chains follows as usual:

$$\frac{d\Psi_n^N}{dt} += k_{rs}\left\{\mu_1\Phi_n^N - (n-1)\sum_{i=0}^{\infty} i^N P_n^i + \lambda_0 \sum_{i=0}^{\infty} i^N \sum_{m=n+1}^{\infty}\sum_{j=i}^{\infty}\left(\frac{P_n^j}{j+1}\right)\right\} \quad (35)$$

For $N = 1$ one obtains the contribution to the first branching moment distribution balance of dead chains:

$$\frac{d\Psi_n^1}{dt} += k_{rs}\left\{\mu_1\Phi_n^1 - \lambda_0 (n-1)\sum_{i=0}^{\infty} iP_n^i + \lambda_0 \sum_{i=0}^{\infty} i \sum_{m=n+1}^{\infty}\sum_{j=i}^{\infty}\left(\frac{P_n^j}{j+1}\right)\right\} \quad (36)$$

Using the same rearrangement as for the living chains we find

$$\frac{d\Psi_n^1}{dt} += k_{rs}\left\{\mu_1\Phi_n^1 - \lambda_0(n-1)\Psi_n^1 + \frac{1}{2}\lambda_0 \sum_{m=n+1}^{\infty}\Psi_m^1\right\} \quad (37)$$

Inserting $N = 2$ and using the same rearrangement as for the living chains, the second branching moment equation follows as

$$\frac{d\Psi_n^2}{dt} += k_{rs}\left\{\mu_1\Phi_n^2 - \lambda_0(n-1)\Psi_n^2 + \lambda_0 \sum_{m=n+1}^{\infty}\left(\frac{1}{3}\Psi_m^2 + \frac{1}{6}\Psi_m^1\right)\right\} \quad (38)$$

Equations 33 and 38 allow the computation of the second moment distributions, which opens the way to finding the broadness of the branching distribution at certain chain length n from Ψ_n^2/Ψ_n^1. However, in the present paper, we will confine ourselves to average numbers of branches per chain, which follow from the zeroth and the first moment. The issue of polydispersity in the branching distributions will be dealt with in future research.

The Final Model in PREDICI. The previous section showed for the ldPE reaction system how the original

Table 2. Kinetic Rate Constants and Other Simulation Input (Mostly taken from Pladis and Kiparissides.[20])[a]

	k_0	E_A [kJ/(kmol K)]	ΔV [m^3/kmol]
k_d [1/s]	5.95×10^{12}	132632	0
η_l [−]	1		
k_p [m^3/(kmol s)]	1.25×10^8	33767	−0.0197
k_{tc} [m^3/(kmol s)]	1.25×10^9	4184	0.013
k_{td} [m^3/(kmol s)]	1.25×10^9	4184	0.013
k_S [m^3/(kmol s)]	$2.62 \times 10^7/3 \times 10^8$ (B)	49664	−0.0197
k_m [m^3/(kmol s)]	$1.25 \times 10^5/4 \times 10^4$ (B)	33767	−0.0197
k_{tp} [m^3/(kmol s)]	4.38×10^8	54936	0.0044
k_{rs} [m^3/(kmol s)]	1.292×10^5	47153	−0.0168
residence time τ (s)		30	
monomer, in (kmol m^{-3})		$M_0 = 16.75$	
initiator feed (kmol m^{-3})		CSTR: $I_{2,0} = 2.47 \times 10^{-5}$	
chain transfer agent, in (kmol m^{-3})		$S_0 = 0.0216/0.48$ (B)	
temperature		260 °C (Alpha), 240 °C (B)	
M_n/M_w (kg/mol): model		26.7/302−668 (Alpha), 12.2/75.2 (B)	
experimental		26/754 (Alpha), 12.2 (B)	
av no. of branches/1000 C: model		1.17 (Alpha), 1.78 (B)	
experimental		1.05 (Alpha), 0.5−2 (B)	

[a] For all CSTR simulations the k_{rs} value shown appears to be the minimum value; some computations have been performed with $4k_{rs}$. Some simulations have been carried out with $2k_{tp}$. "Alpha" refers to comparison with Tackx and Tacx.[1] "B" denotes the slightly different kinetic data used when comparing model to Borealis data.[6]

bidimensional MWD/DBD problem can be reduced to a unidimensional problem in a straightforward way. For the DBD only the first moment is computed, which can be done without any further assumption or closure relationship. Now, having derived the balance equations for reduced distributions for all reaction steps, and adding the equations for the real distributions as well as the balance equations for the low molecular species and the relevant initial and feed conditions for CSTR and batch reactor, our model is complete. The pseudo distributions are treated by PREDICI in an identical manner as the real distributions, and thus are readily implemented. This model is available now and has been tested against experimental data as described below. This is an important achievement in the field of distribution modeling, since provided the set of reaction mechanisms is complete and correct, and the kinetic rate constants are correct, the MWD and DBD obtained are beyond doubt, because no important assumptions are made in between. Reversely, this means that any possible discrepancies between modeled and experimental MWD and DBD must be attributed either to an incorrect description in terms of reaction mechanisms and kinetic data or to experimental errors.

Rate Constants

The rate constants used in our study are listed in Table 2. They are almost identical to recently published ones.[20] Propagation, termination, and some transfer rate constants are becoming available as more and more accurate and reliable data are provided by such modern techniques as pulsed laser SEC.[16] It is known that the system's behavior is especially sensitive to the ratios k_p/k_t^2, k_m/k_p, and k_s/k_p. With these ratios, the model is tuned to the relevant conversion (12−18%) and M_n (12−27 kg/mol) range. For the modeling of MWD and DBD, the ratios k_{tp}/k_p and k_{rs}/k_p are extremely critical. The k_{tp} may be inferred from DB data in a fairly straightforward way as long as the averaging is carried out correctly, as explained in the previous section. Thus, the order of magnitude of k_{tp}/k_p is found to be 0.01. There is no such direct method for obtaining k_{rs}, which therefore has to be deduced from the measured MWDs and DBDs. As will be discussed in the section about the simulation results (Figures 9 and 10), we varied the random scission rate in order to observe its influence

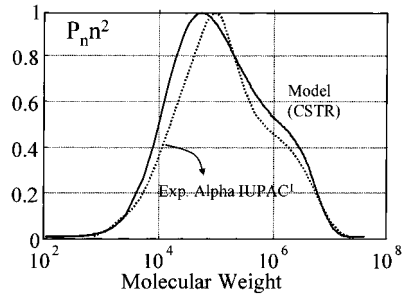

Figure 1. Comparison of MWD from model and SEC/MALLS measurements of autoclave product Alpha IUPAC[1] data (experimental values estimated from MWD plot): M_n (expt) = 29, M_n (model) = 26; M_w/M_n (expt) = 26, M_w/M_n (model) = 25; conversion (model) = 18%, temperature 260 °C. Model MWD is obtained using kinetic data from open literature[20]—except for a factor of 100 lower k_{rs}—and for the simplest reactor type: ideal CSTR with uniform temperature. Effect of higher k_{rs} goes from Figure 10.

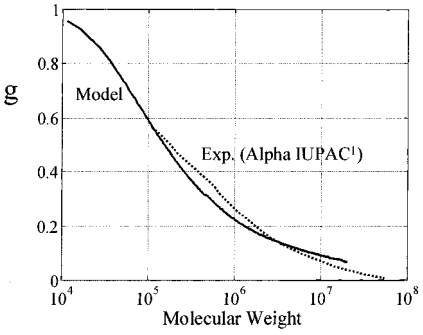

Figure 2. Comparison of gyration radius g as calculated from the simulated branching distribution for a CSTR from eq 39 and a directly measured (MALLS[1]) g for autoclave product Alpha IUPAC. Good agreement between autoclave product data and model, the latter showing slight underestimation for MW < 1.5×10^6 and overestimation beyond.

on the MWD shape. For a k_{rs}/k_p value of 5×10^{-5}, good agreement has been found between the simulated and the experimental[1] MWD. For a CSTR, this shape turned out to be very sensitive to k_{rs}: Higher values removed the shoulder altogether and narrowed the MWD, and lower values failed to yield a converged solution. Note that the value mentioned is a factor 100 lower than that used by Pladis and Kiparissides.[20]

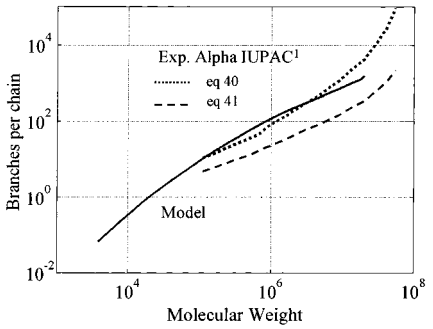

Figure 3. Comparison of branching distribution from CSTR model, corresponding to MWD of Figure 1, and the gyration radius data[1] shown in Figure 2. Good agreement for the autoclave CSTR model is observed, in line with Figure 2.

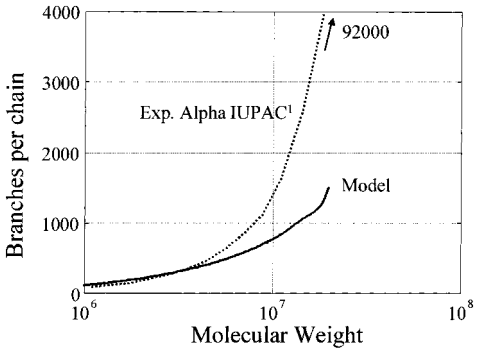

Figure 4. Close up of Figure 3 at high MW end and on linear branching number scale. Model and autoclave data have good agreement until MW = 10^7 kg/mol. Experimental curve ends at around 92 000 branches per chain, while the model predicts a maximum of 1500.

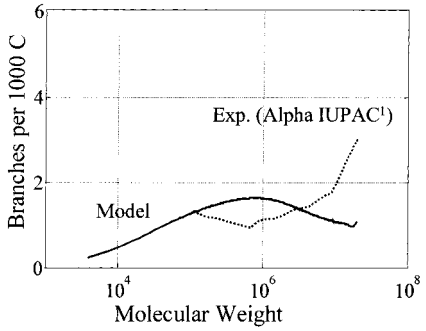

Figure 5. Comparison of branching density from model and SEC/MALLS measurements of Alpha IUPAC,[1] corresponding to MWD of Figure 1. Average branching density: 1.17/1000 C (model); 1.05/1000 C (experimental, estimated from g plot, using eq 40; when using the equation for polydisperse systems, eq 41, a lower value is obtained: 0.52/1000 C).

Comparison of Model Outcomes with Experimental Data

Molecular Weight and Degree of Branching Distribution Data. Nonconfidential measured MWD data are only scarcely available; some are recent[1] and some are less recent.[2,4] The relevant M_n and polydispersity ranges are M_n around 10−30 kg/mol and polydispersities for tubular reactors 3.5−12 and autoclaves 10−25. MWDs from size exclusion chromatography essentially measure the hydrodynamic volume of the molecules. The interpretation of these data yielding the concentration is straightforward. However, the relation between hydrodynamic volume and MW depends on the degree of branching: The more highly branched, the smaller the volume for a given MW. Hence, SEC calibrated for linear chains underestimates the MW of branched chains; in other words, SEC cannot sharply fractionate in MW a product with a distribution in number of branches per chain. Such techniques as low-angle or multiangle laser light scattering (MALLS) offer the possibility to directly determine the size of the molecule. This information is used to correct the SEC data for the branching effect, so that a proper MWD is obtained.

Evidently, the same or similar combinations of techniques are used to obtain the DBD itself. It requires a

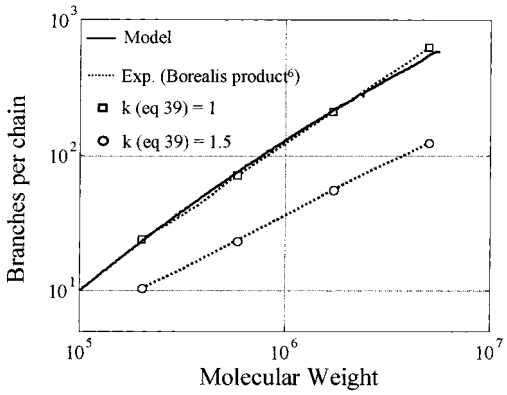

Figure 6. Comparison of experimental DB data for Borealis product[6] (two values for exponent k in eq 39) to simulations of CSTR model (identical kinetic data and M_n = 12.2 kg/mol, T = 240 °C; M_w = 75.2 kg/mol). Excellent agreement for k = 1 in eq 39 is observed.

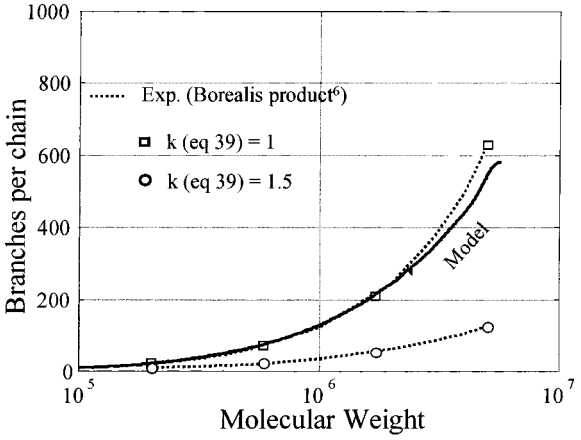

Figure 7. Comparison on DBD of Borealis experimental data[6] [to = with] model simulations. Same as Figure 6, but on a linear DB scale.

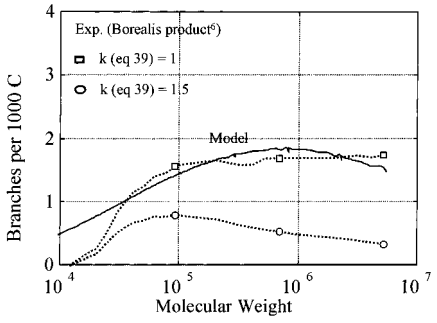

Figure 8. Comparison of experimental branching density data from Borealis[6] (2 values for exponent k in eq 39) [to = with] simulations. Discrepancy at lower MW, but accuracy of experimental data falls at low MW. Average branching density: 1.78/1000 C (model), 1.7/1000 C (experimental, estimated from g' plot).

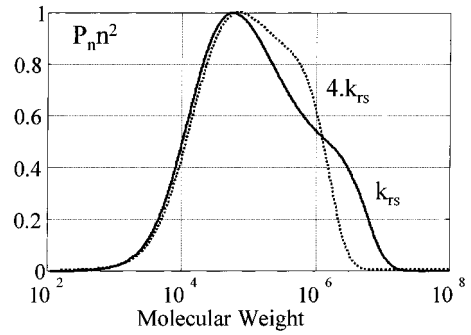

Figure 9. Effect of random scission rate on MWD in a CSTR. Identical conditions as in Figure 1. Bimodality almost vanishes and MWD becomes considerably narrower: Polydispersity decreases from 25 to 10. Average degree of branching remains unchanged.

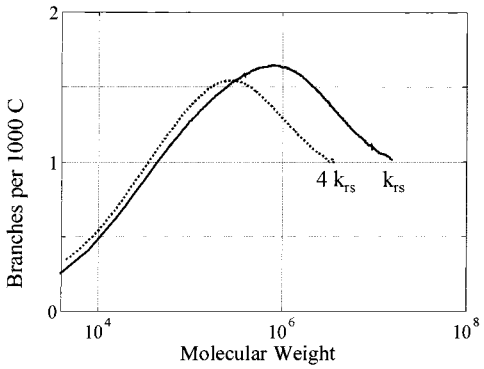

Figure 10. Branching density for ldPE from model (bimodal MWD and narrower MWD for stronger random scission, see Figure 9). Clear maximum observed. Stronger random scission shifts the curve to lower MW, indicating a 'redistribution' of branches over shorter chains.

number of steps, assumptions, and models to transform the data into a number of branches per chain.[21,22] One important assumption is contained in the well-known formula relating the structural parameter g'—which denotes the ratio between the intrinsic viscosities of branched and linear molecules of the same MW—and g, which denotes the ratio of square gyration radii of branched and linear molecules of the same MW:

$$g' = g^k \tag{39}$$

The ratio g is directly coupled to the number of branches in a chain according to relationships derived by Zimm and Stockmeyer[34] for various cases. For the case of a sample with uniform chain lengths and a uniform number of branches per chain i, and hence *monodispersity* in both distribution dimensions, the formula for g is

$$g(i) = \frac{\langle s^2\rangle_{br}}{\langle s^2\rangle_l} = \frac{3}{(f-1)i+3}\left[1 + \sum_{j=1}^{i}(f-1)^j \prod_{m=0}^{j-1}\left\{\frac{i-m}{(f-1)i+2-m}\right\}\right] \tag{40}$$

Here, f denotes the branching functionality, for ldPE taken as 3. Note that $g(i)$ is independent of chain length. Using eq 40, one may calculate the number of branches i when $g(i)$ is known; for instance, if $g = 0.5$, the number of branches is 16. Now, a problem arises from the fact that SEC fractionates according to *hydrodynamic volume*. Since, in agreement with eq 40, branched molecules have smaller sizes and volumes at the same weight, the SEC fractions will contain certain ranges of MWs and DBs. Hence, the assumption of ideal monodispersity does not apply to the full extent. Some authors therefore use an alternative relationship[34] that applies to *complete* populations containing all MWs and DBs:

$$g(n) = \frac{6}{n_w}\left[\frac{1}{2}\left\{\frac{(2+n_w)^{0.5}}{n_w^{0.5}}\ln\left(\frac{(2+n_w)^{0.5}+n_w^{0.5}}{(2+n_w)^{0.5}-n_w^{0.5}}\right)\right\} - 1\right] \tag{41}$$

Since we believe that monodispersity is closer to reality, eq 40 is used to interpret experimental branching data. However, modeling efforts are currently being made[28] to predict radii of gyration from DB accounting for the *architecture* of the molecules. In future publications, we will report on the development of our own tools designed to improve the predicting of rheological properties and molecular size distributions from explicit molecular architectures.

Tackx and Tacx[1] have determined g directly from SEC/MALLS experiments on ldPE, from which the branching has been determined using eq 40. All less recent sources yield experimental data in terms of g', thus eq 39 and a value for k is needed to obtain g. The exponent k is a highly disputed parameter, since for ldPE values between 0.5 and 1.5 have been reported.[22] Values have been reported[1] of $k = 1-1.5$ for one-zone autoclave ldPE and of $k = 1.25-2$ for tubular ldPE. In our study, we use k as a parameter with values of either 1 or 1.5 in the comparison to experimental data, except of course when comparing with g data.[1] The literature contains only scarce data concerning DB distributions[6] and averages.[32] The order of magnitude of DB is typically around 1−2 branches per 1000 C in recent publications,[1,6] but has been reported to be as high as 12 in older ones.[32]

Comparison between Model Predictions and Measurements. The model outcomes will be compared to experimental MWD data from one and to DBD data from two sources that provide autoclave product data: Tackx and Tacx[1] and Nordhus et al.[6] Regarding the comparison, it should be noted that a single, isothermal CSTR is not a highly realistic representation of a real autoclave configuration. However, it will become clear that the peculiar shape of the broad MWD is already fully there in the simple CSTR, while not being strongly modified by mixing effects as modeled by systems of CSTRs with recirculation.[13]

Tackx and Tacx[1] provide measurement data for MWDs and values of g vs molecular weight for one zone autoclave ldPE, a bimodal product denoted by Alpha IUPAC. The MWD is measured using MALLS to obtain the average mass per SEC fraction and using refractrometry for the concentration. Hence, the molecular mass is determined *directly* without requiring any correction for branching, which would have been necessary had viscosimetry been used, yielding hydrodynamic volume rather than mass.

Molecular Weight Distribution. The measured MWD of Alpha IUPAC (simply reproduced from the reference) is compared to the MWD predicted by our PREDICI model for an ideal CSTR in Figure 1. The

agreement is remarkable, considering the reactor conditions for Alpha IUPAC are far from ideal and of uniform temperature, and for obvious reasons are not mentioned by the authors. It should also be borne in mind that the kinetic data set used is from open literature,[20] except for the fitted random scission rate. The agreement found, and especially the reproduction of the bimodal MWD by the model, is strong support for the validity of our model. This MWD shape is only obtained in a CSTR and within a very narrow range of the random scission rate factor. This is confirmed by the sensitivity study regarding k_{rs} at the end of this section. Therefore, we conclude that the subtle interplay between all kinetic mechanisms and residence time distribution leads to a marked dominance of the bimodal shape that is relatively weakly influenced by nonidealities and segregation effects. Evidently, when details of such effects become available from information on the process conditions for Alpha IUPAC, improved fine-tuning using models accounting for segregation will become feasible as well. Note that the agreement between model and experiment[1] is completely based on the visual comparison of the MWDs. Since the experimental reference does not provide M_n and M_w values, a precise check of the simulated values (26.7 and 668 kg/mol, respectively) is not possible. However, the MWD shape presented is no reason to change the rates of transfer to monomer and solvent as determining factors for the M_n. This, in part, is related to the difficulties involved when attempting to infer an accurate M_n value from an MWD measured using SEC.

Degree of Branching Distribution. To start with, in Figure 2 the direct MALLS measurement data of square radius of gyration g are compared to our model results for a CSTR, using eq 39 to obtain g from number of branches per chain. The agreement is good, although experimental data extend over a somewhat longer range. According to the model predictions, the ranges of g are exactly the same as those for MWD, ending at slightly above 10^7 g/mol. The experimental MWD confirms this (see Figure 1). However, the g curve extends to 10^8 kg/mol. This means that the experimental technique for detecting branches (MALLS) reveals the existence of extremely long, strongly branched molecules with too low concentrations to be detected by the refractometer. As a hypothetical explanation, we think that this is due to the existence of a small fraction of very long, highly branched chains that are undetectable by the refractometer but detectable by MALLS in the most sensitive range of this instrument.

In Figure 3, experimental DBD data are compared to the predicted ones in terms of number of branches per chain (data obtained from the shown g measurements and eq 40). The number of branches per chain increases with chain length, which is intuitively in agreement with the fact that the transfer to polymer reaction rate is proportional to the length of the dead chains. The agreement between experiment and model is again good, but in Figure 4 at high MW the number of branches per chain amounts to 92 000, whereas the model predicts a maximum of only 1500. The value of 92 000 seems to be extremely high and gives rise to some doubt. In the first place, it had to be estimated from an experimental g plot[1] in a region where $g < 0.01$, so that the accuracy of both the instrument's output signal and the plot is low. Moreover, it should be noted that an interpretative model is still needed to translate g into number of branches. For reasons already explained, we used eq 40 (monodisperse sample) as this model; however, using eq 41 (full polydisperse population) would have resulted in far fewer branches per chain, a better fit at high MW, and a worse fit at lower MW as compared to our simulation model (see Figure 3). More experimental data and improved interpretative models are needed in order to arrive at a full understanding of this matter. Figure 5 shows the branching density vs MW, showing a maximum in the computed curve, which is absent from the experimental one; in contrast, the latter shows a minimum and a remarkably sharp increase at high MW, but this is subject to some doubt, as explained above. The average branching density can be calculated from the measured g data as follows. Experimental g values are known as a function of MW. Through either eq 40 or eq 41, the number of branches i per chain is obtained from $g(i)$, yielding the number of branches as a function of MW. The concentration distribution of MW is known from the experimental MWD, so the total number of branches follows by integration over the whole MW range. Dividing the total number of branches by the total number of chains, as obtained from the experimental concentration, yields the average number of branches per chain. Finally, dividing the total number of branches by the total number of monomer units in all the polymer chains (from experimental MWD) provides us with the number-average branching density. This average turned out to be 1.05 branches/1000 C (eq 40), which is close to the predicted value of 1.17/1000 C; using eq 41 yielded a larger discrepancy, i.e., 0.52/1000 C. The existence of a maximum in the branching density curve is not expected intuitively. Since every unit on a dead chain—whether short or long—has the same chance of being attacked by the transfer to polymer reaction, one might anticipate that the branching density is also independent of chain length. This, however, turns out to be incorrect, which is a result of the complex interplay between all mechanisms involved.

Nordhus et al.[6] presented measured g' curves for various autoclave grades produced by Borealis. From these data, they calculated branching data using the Zimm and Stockmeyer[34] formula for polydisperse systems (eq 41), so in line with the discussion above, we have reworked the g' data using eq 40, which holds for monodisperse systems. As regards MWD, unfortunately this reference does not show the corresponding MWD *measurements*, but only computed ones, assuming three CSTRs in series.

Degree of Branching Distribution. The same kinetic set as before has been used, except for different transfer rates to monomer and solvent (see Table 2). The CTA concentration in the Borealis case is unknown. It turned out that a value of 0.48 kmol/m^3 leads to an excellent agreement between model and data, as seen in Figures 6 and 7, when assuming $k = 1$ in eq 39 as regards the interpretation of the experimental results. Figure 8 shows the branching density of the Borealis product resulting from experiments and model, again revealing an excellent agreement. Discrepancies are observed at lower MW, probably due to less sensitivity and accuracy of the measurement instrument in this range.

Some Simulations with the ldPE Model. The effect of a higher random scission rate is shown in Figure 9. A further reduction of this rate leads to a

divergence: The model shows that especially living chains continue to grow and do not reach steady state. Our hypothesis is that, in the absence of random scission, transfer to polymer will lead to gelation, which is an infeasible region for our model. We conclude that the MWD is strongly affected by random scission, and hence the shape of the MWD may be seen as a sensitive, quantitative measure of random scission. Note that this conclusion only holds for a CSTR, since batch reactor calculations not reported here show the MWD sensitivity for random scission to be much lower. At present, it is possible to simulate more realistic reactor configurations of autoclave and tubular systems using the PREDICI in compartment models in order to allow for mixing effects and nonisothermal conditions.[13]

Although discrepancies still persist between the model based on the kinetic scheme presented and the experimental DBD data—especially with respect to the shape of the DBD curves—it nevertheless seems interesting to analyze typical bimodal autoclave products on branching characteristics. These DBD results are given in Figure 10 as branching density characteristic. The average number of branches per chain is not affected by random scission, in line with the principles of this mechanism. However, the effect of higher random scission is a kind of redistribution of the branches created by transfer to polymer over a lower MW range, which is clearly visible in Figure 10.

Discussion and Conclusions

The use of pseudo distributions in PREDICI has proven to be a rigorous and powerful simulation tool with which to obtain the degree of branching distributions on a reactor level of aggregation. The only compromise made to rigorousness concerns the implementation of random scission. Complete decoupling of chain length and number of branches scission allowed us to include this mechanism in the pseudo distribution approach. The inherent overestimation of number of branches in short chain fragments (as discussed in the Appendix) introduces an error of less than 1%. For the reaction mechanisms assumed and the kinetic rate data given in Table 2, the DBD obtained is correct. Obviously, this conclusion holds for the description of the first moment of the DBD at a certain chain length. However, as real bidimensional distribution modeling of MWD/DBD on reactor scale is not yet possible, the results obtained using pseudo distributions should be considered the state of the art in rigorousness. Furthermore, although no experimental data are available on DBD per chain length, we may anticipate that these distributions are neither broad nor of a very particular shape, so that the moment approach is safe here. Note that Zimm and Stockmeyer[34] even had a Poisson distribution in mind. Still, PREDICI offers the possibility to incorporate higher moment pseudo distributions, something we will undertake in the future.

Model results have been compared to experimental data from several sources. A number of interesting results have been obtained. By assuming a set of kinetic data from available literature,[20] we were able to simulate the typical bimodal MWD as measured for ldPE from autoclave reactors.[1] Moreover, the MWD shape turns out to be a sensitive measure for the random scission rate, at least for CSTR type reactors.

For DBD, good agreement is found between our CSTR model using kinetic data from open literature and the available experimental data for Alpha IUPAC[1] and a Borealis[6] product. This is even more remarkable in view of the accuracy of measured DBD[1,5,6] as obtained from SEC-MALLS data, since the interpretation of such data requires to make a number of assumptions that render them not completely unambiguous. The maximum number of branches found by our model is lower compared to the first reference (1500 rather than 92 000) and the same (600) in the latter case. A difference is observed in the branching density, predicted to feature a maximum (1.75 branches per 1000 C), but in the Alpha IUPAC case it is seen to show a sharp increase to 25 branches per 1000 C at high MW according to experimental data. The extremely high experimental values are subject to some doubt for reasons of instrumental accuracy and the accuracy with which the interpretative model can translate g into number of branches. The sharp increase is not at all observed in the Borealis autoclave product, where the agreement between branching density data and model predictions is almost perfect. In general, the discrepancies still present may be partly ascribed to segregation or micromixing effects, phenomena which may be investigated using our model.[14] Eventually, differences could also be explained by incorrect kinetic coefficients, but only very partially, so such an explanation is unsatisfactory. However, it is still an open question to what extent some mechanisms included in the model should be modified or refined: Is the rate of transfer to polymer really proportional to the chain length, and is random scission really random? These issues deserve closer examination.

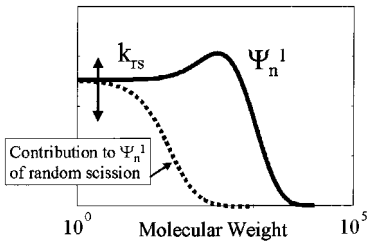

Figure 11. Plateau shape of Ψ_n^1 distribution toward low n. This is due to the high fraction of random scission in the production of Ψ_n^1 at low n. Since also the P_n distribution has a plateau at low n, the branching density 500 $\Psi_n^1/(P_n n)$ assumes unrealistically high values.

Appendix: Special Features of Random Scission

In this appendix the impact of random scission on the pseudo distribution Ψ_n^1 is discussed, especially with respect to the complete decoupling between scission into chain lengths and scission into branching numbers as described in the main text.

Some calculated pseudo distributions Ψ_n^1 have been examined more closely. For broad MWD, the associated Ψ_n^1 distribution turns out to possess a plateau at short chain lengths, as shown in Figure 11. Analyzing the contributions of all reaction mechanisms involved, it appears that random scission dominates at low n. As can be seen from Figure 11, the fraction of Ψ_n^1 being a product of random scission is almost 100% at low n and gradually decreases to zero at higher n. In conclusion, the plateau in Ψ_n^1 is caused by random scission. Now, since the dead chain distribution P_n also features a plateau at low n, the quotient Ψ_n^1/P_n (the number of branches per chain at length n) will approach a constant value at low n. Finally, it follows that the branching density, computed as 500 $\Psi_n^1/(P_n n)$ representing the

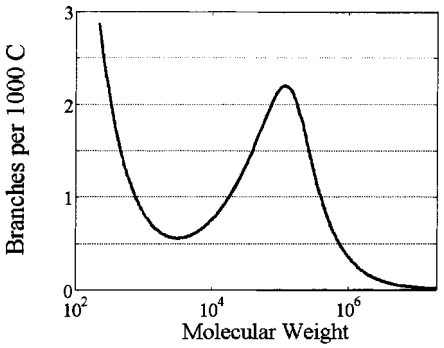

Figure 12. Branching density 500 $\Psi_n^1/(P_n n)$ vs molecular weight. The sharp rise toward low n is a consequence of the plateau shape of the Ψ_n^1 distribution at low n shown in Figure 11. As argued in the text, the overestimation of the branching density is negligible for $n > 100$, or MW > 3000.

number of chains per 1000 C, rises considerably toward low n. This is shown in Figure 12. Physically, this is unrealistic and must be explained by the aforementioned overestimation of branches created in very short chains by random scission, due to the incorrect summation in the expression for the pseudo distribution describing the contribution of this mechanism. As stated, the error is only significant if the orders of magnitude of chain length and number of branches are the same. Knowing that, up to chain lengths 100, the average number of branches per chain is lower than one, we assume that the error has become negligible beyond that length. Moreover, since the experimental techniques are not able to detect branches below $n = 300$ ($M_n = 10\,000$), this error is not relevant when comparing simulations with experimental data. Theoretically, the overestimation of branches in short fragments has its corollary in an overestimation of the consumption of branches from long chains. However, since only a small fraction of the chains is broken into very short chains, this error—being proportional to that fraction—may safely be neglected.

Nomenclature

B	total number of branch points (−)
E_A	activation energy in Arrhenius expression (kJ (kmol·K)$^{-1}$)
g	ratio of square radii of gyration of polymers with the same molecular weight (−)
g'	ratio of intrinsic viscosities of polymers with the same molecular weight (−)
I_2, I	concentration of undissociated and dissociated initiator, respectively (kmol m^{-3})
k	exponent in eq 39, rate constants in Tables 1 and 2 (−)
k_0	preexponential factor in Arrhenius expression (−)
M	monomer concentration (kmol m^{-3})
M_n, M_w	number and weight-average molecular weights, respectively (kg kmol^{-1})
n_w	weight-average segment length in eq 41 (−)
P_n^i	concentration of dead chains with length n and number of branches i (kmol m^{-3})
R_n^i	concentration of living chains with length n and number of branches i (kmol m^{-3})
s	radius of gyration (m)
S	solvent concentration (kmol m^{-3})
ΔV	activation volume in Arrhenius expression (m^3/kmol)
β	probability that a chain of length m with j branches produces a fragment of length l with k branches (−)
Φ_n^N	Nth branching moment of living chains with length n (kmol m^{-3})
Ψ_n^N	Nth branching moment of dead chains with length n (kmol m^{-3})
τ	residence time in reactor (s)

References and Notes

(1) Tackx, P.; Tacx, J. C. J. F. *Polymer* **1998**, *39*, 3109−3113.
(2) Kuhn, R.; Kromer, H.; Rosmanith, G. *Angew. Makromol. Chem.* **1974**, *40*, 361.
(3) Scholte, Th. G.; Meijerink, N. L. J. *Br. Polym. J.* **1974**, *133*, 9.
(4) Luft, G.; Kämpf, R.; Seidl, H. *Angew. Makromol. Chem.* **1983**, *111*, 133.
(5) Axelson, D. E.; Knapp, W. C. *J. Appl. Polym. Sci.* **1980**, *25*, 119.
(6) Nordhus, H.; Moen, O.; Singstad, P. *J. Macromol. Sci.—Pure Appl. Chem.* **1997**, *A34*, 1017.
(7) Biesenberger, J. A.; Sebastian, D. H. *Principles of Polymerisation Engineering*; Wiley: New York, 1983.
(8) Chan, W.-M.; Gloor, P. E.; Hamielec, A. E. *AIChE J.* **1993**, *39*, 111−126.
(9) Daniels, W. Vinyl Acetate Polymers. In *Encyclopaedia of Polymer Science and Technology*, 1st ed.; Wiley, New York, 1989; Vol. 17, pp 402−425.
(10) Hulburt H. M.; Katz, S. *Chem. Eng. Sci.* **1964**, *19*, 555−574.
(11) Hutchinson, R. A.; Fuller, R. E. *6th International workshop on Polymer Reaction Engineering, Berlin* **1998**; DECHEMA Monographs 134; Wiley-VCH: Weinheim, Germany, 1998; pp 35−48.
(12) Iedema, P. D.; Hamersma, P. J.; Hoefsloot, H. C. J. *6th International workshop on Polymer Reaction Engineering Berlin* **1998**; DECHEMA Monographs 134; Wiley-VCH: Weinheim, Germany, 1998; pp 661−677.
(13) Iedema, P. D. *VIII Ogólnopolskie Seminarium MIESZANIE (Mixing Conference)*, Warsaw **1999**; ISSN 1234−4354, pp 115−121.
(14) Kiparissides, C.; Verros, G.; MacGregor, G. F. *J. Macromol. Sci.—Rev. Macromol. Chem. Phys.* **1993**, *C33*, 437−527.
(15) Laemmel, R. Ph.D. Dissertation, University of Goettingen, 1996.
(16) Mead, D. W. *J. Appl. Polym. Sci.* **1995**, *57*, 151−173.
(17) Nagasubramanian, K.; Graessley, W. W. *Chem. Eng. Sci.* **1970**, *25*, 1549−1558.
(18) Nagasubramanian, K.; Graessley, W. W. *Chem. Eng. Sci.* **1970**, *25*, 1559−1569.
(19) Tefera, N.; Weickert, G.; Westerterp, K. R *J. Appl. Polym. Sci.* **1997**, *63*, 1663−1680.
(20) Pladis, P.; Kiparissides, C. *Chem. Eng. Sci.* **1998**, *53*, 3315−3333.
(21) Rudin, A.; Grinshpun, V.; O'Driscoll, K. F. *J. Liq. Chromatogr.* **1984**, *7*, 1809−1821.
(22) Shiga, S. *Polym.-Plast. Technol. Eng.* **1989**, *28*, 17−41.
(23) Teymour, F.; Campbell, J. D. *Macromolecules* **1994**, *27*, 2460−2469.
(24) Tobita, H.; Hatanaka, K. *J. Polym. Sci., Part B: Polym. Phys.* **1996**, *34*, 671−681.
(25) Tobita, H. *Macromolecules* **1996**, *29*, 3000.
(26) Tobita, H. *Macromolecules* **1996**, *29*, 3010.
(27) Tobita, H. *Macromol. Theory Simul.* **1998**, *7*, 225−232.
(28) Tobita, H.; Saito, S. *Macromol. Theory Simul.* **1999**, *8*, 513−519.
(29) Triacca, V. J.; Gloor, P. E.; Zhu, S.; Hrymak, A. N.; Hamielec, A. E. *Polym. Eng. Sci.* **1993**, *33*, 445−454.
(30) Villermaux, J.; Blavier, L. *Chem. Eng. Sci.* **1984**, *39*, 87.
(31) Wulkow, M. *Macromol. Theory Simul.* **1996**, *5*, 393−416.
(32) Yamamoto, K. *J. Macromol. Sci.—Chem.* **1982**, *A17*, 415−431.
(33) Zabisky, R. C. M.; Chan, W.-M.; Gloor, P. E.; Hamielec, A. E. *Polymer* **1992**, *33*, 2243−2262.
(34) Zimm, B. H.; Stockmeyer, W. H. *J. Chem. Phys.* **1949**, *17*, 1301−1314.
(35) Zhu, S.; Hamielec, A. E. *J. Polym. Sci., Part B: Polym. Phys.* **1994**, *32*, 929−943.

MA991711O